Reliability analysis of grid-interfaced filter capacitors

Zhou, Dao; Wang, Haoran; Wang, Huai; Blaabjerg, Frede

Published in:
Chinese Journal of Electrical Engineering

Publication date:
2018

Document Version
Publisher's PDF, also known as Version of record

Reliability Analysis of Grid-Interfaced Filter Capacitors

Dao Zhou, Haoran Wang, Huai Wang, and Frede Blaabjerg*

(Department of Energy Technology, Aalborg University, Aalborg, 9220, Denmark)

Abstract: Growing with the increased adoption of renewable energy for the power generation, the reliable and cost-effective operation of grid-connected inverters is of more and more importance. A filter is interfaced between an inverter and the utility grid to reduce the switching harmonics. According to the modulation scheme and the LCL filter impedance, the electrical stresses of the filter capacitor can be thoroughly investigated. With the help of the electro-thermal model, its long-term thermal stress can be obtained based on the mission profile like wind speed, ambient temperature. The reliability of the filter capacitor bank is obtained based on its individual capacitor reliability curves and reliability block diagram method. A case study on a 2MW wind turbine system demonstrates the relationship between the lifetime of the capacitor bank and the single capacitor. Moreover, the severe voltage and current stresses of the filter capacitors are analyzed during abnormal operations (e.g., fault ride-through) with asymmetrical parasitic parameters.

Keywords: Metalized polypropylene film capacitor, reliability, doubly-fed induction generator, fault ride-through.

1 Introduction

With the increased adoption of renewable energy for the power generation, the three-phase voltage source inverter has become an important interface to convert clean energy to the utility grid[1]. A filter is usually required in between to introduce a current feedback control. A single inductor L filter can be used, but the harmonic attenuation may not be sufficient. A high voltage drop is produced due to the bulky inductor. Especially in the high-power application, where the switching frequency is always limited by the associated switching losses, such a simple configuration may lead to the costly passive filter and slow down the system dynamic response[2] Commonly, a high-order LCL filter is used, as it achieves a higher attenuation along with the weight saving of the components. The smaller inductor and capacitor used in the LCL filter minimizes the amount of current harmonics injected into the utility grid, which complies with the harmonic standards.

The performance of capacitors is highly affected by its operational conditions such as the voltage, current, frequency, and temperature. Many researchers have investigated the degradation of the electrolytic capacitors[3-7]. For instance, a real-time failure detection method is developed by estimating the changes in its Equivalent Series Resistance(ESR) and capacitance[5]. Lifetime prediction models of electrolytic capacitors are established for the switch-mode power supplies and variable-frequency drivers[6-7]. However, few studies investigate the reliability analysis of the film capacitor considering mission profile[8], and this paper develops the approach to evaluate the reliability of the capacitors in the grid-interfaced filter. Moreover, it is a physics-of-failure approach[9] from the component-level to system-level reliability that based on electro-thermal modeling, lifetime modeling, Weibull analysis, and reliability block diagram.

The structure of this paper is organized as follows: Section 2 describes the design criteria and failure mechanism of the filter capacitor. Electrical stresses of the filter capacitor are presented in Section 3. According to the mission profile based lifetime prediction of the individual capacitor. Section 4 presents the time-to-failure of individual capacitors and the lifetime of the filter capacitor bank. Section 5 evaluates impact of asymmetric parasitic parameters on the filter capacitor stress under grid faults. The concluding remarks are drawn in the last section.

2 Design criteria and failure mode of filter capacitor

As shown in Fig.1, the grid-connected inverter is widely used in renewable energy systems. Due to the switching harmonic introduced by the Pulse Width Modulation(PWM) inverter, a filter is usually applied in between to limit the corresponding harmonic current flowing into the grid[10].

As the LCL filter features as higher impedance at switching-frequency range compared to the single L filter, it is a preferred solution used in the grid-connected inverter. The design procedure of the LCL filter is described in [11], the inverter-side inductor is selected according to the current switching ripple requirement,

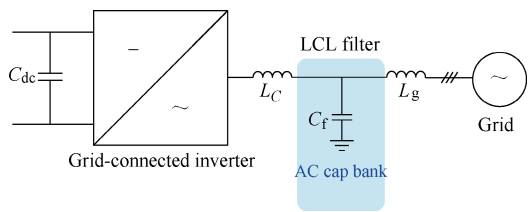

Fig.1 Configuration of a grid-connected inverter with an LCL filter

* Corresponding Author, E-mail:zda@et.aau.dk.

while the grid-side inductor is chosen on the basis of the harmonic specification from the IEEE standard. For the filter capacitor, it is designed as seen from the additional introduced reactive power. As larger capacitance causes higher current stress of the power component and higher loss dissipation, 5%~10% of the absorbed reactive power at the rated operation condition is the rule- of-thumb[11].

It is well known that various types of capacitors are used in power electronic converters. Electrolytic capacitors are applied in the case of the high capacitance per volume(e.g. DC-link applications). Due to the polarity, the film capacitors are used in the grid filter owing to the high electric-field stress. Moreover, the material of polypropylene is preferred as compared to polyethylene terephthalate, because of the much lower loss factor. One of the main failure modes is caused by the high capacitor temperature and high current, which leads to a reduced breakdown voltage and even melting of the capacitor.

3 Capacitor performance under normal grid condition

Based on the modulation scheme of the power converter, this section starts to analyze electrical stresses (e.g. the ripple current, and voltage) of the filter capacitor with the help of the LCL filter impedance modeling. In the case of a Doubly-Fed Induction Generator(DFIG) based wind power generation, the impact of loading conditions on capacitor electrical stresses is investigated and evaluated.

3.1 Electrical stresses of filter capacitor

In order to evaluate the current flowing through the filter capacitor, it starts with the analysis of the converter voltage. According to the impedance characteristics of the LCL filter, both the converter-side current and the grid-side current are analyzed, and the capacitor current is also calculated.

For the three-phase system, the space vector modulation(SVM) is preferred compared to the Sinusoidal Pulse Width Modulation(SPWM) due to its higher DC-link voltage utilization. The duty cycle of the two adjacent non-zero vectors (d_1, d_2) and the zero vectors (d_0) can be obtained at different sectors,

$$\begin{cases} d_1 = \dfrac{\sqrt{3}}{2} M \sin\left(\dfrac{k\pi}{3} - \varphi_u\right) \\ d_2 = \dfrac{\sqrt{3}}{2} M \sin\left(\varphi_u - \dfrac{(k-1)\pi}{3}\right) \\ d_0 = 1 - d_1 - d_2 \end{cases} \tag{1}$$

where k denotes the sector number; M denotes the modulation index ($0 \leqslant M \leqslant 1.15$), which equals to the inverter peak voltage over a half of the DC-link voltage V_{dc}; φ_u denotes the phase angle of the inverter voltage.

As shown in Fig.2(a), six sectors (Sector 1 to 6) can be divided in accordance with the phase angle of the inverter voltage φ_u. In the case of Sector 1, the voltage vector V_o is composed of two adjacent active vectors V_1(100) and V_2 (110) (with duration periods of T_1 and T_2 within the switching period T_s), as well as two zero vectors V_0 (000) and V_7 (111) (with duration period of T_0 within the switching period T_s). Both the active and zero vectors are symmetrically arranged in order to achieve the minimum harmonics of the output voltage[12]. The possible switching patterns of the power devices are described in Fig.2(b) in details. Due to the symmetrical loading of the three-phase system, the inverter voltage V_{ao} is illustrated in Fig.2(c). Depending on the various switching states of the power devices, it can be seen that

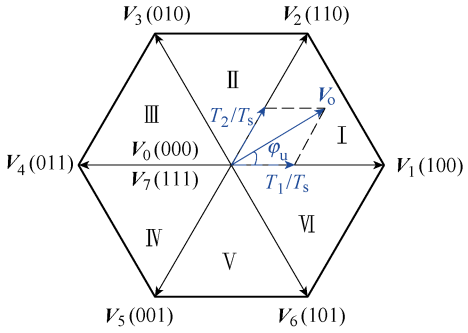

(a) Six sectors

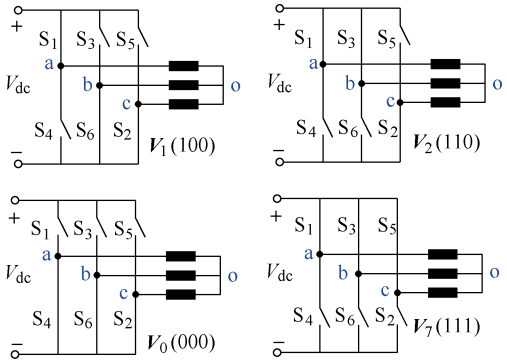

(b) Switching states existing in Sector 1

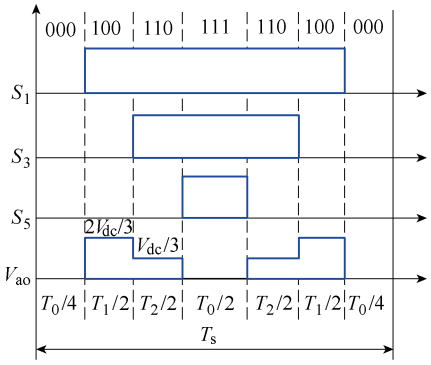

(c) Phase voltage of converter output in Sector 1

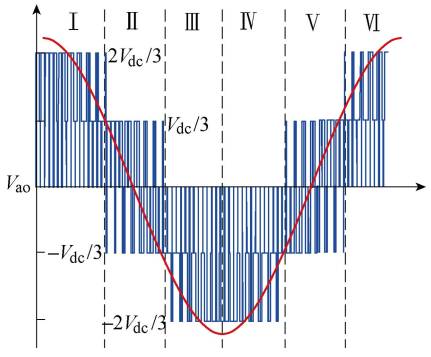

(d) Phase voltage of the converter output within a fundamental period

Fig.2 Illustration of space vector modulation

the output voltage includes the levels of $2V_{dc}/3$, $V_{dc}/3$, and 0. By using the similar approach, the inverter voltage waveform can be obtained in the other five sectors, which contains three voltage levels within the same sector as described in Fig.2(d).

In order to obtain the fundamental and harmonic components of the converter voltage, the Fourier analysis is employed. Based on the impedance characteristics of the LCL filter, the electrical stresses of the filter capacitor are calculated. For a pulse voltage, its Fourier coefficient is calculated by its starting and ending time instants together with its voltage amplitude[12]. Since 7 pulse voltages exist within a switching period, the Fourier coefficient is summed up together with the duty cycle and its corresponding voltage amplitude. With the voltage amplitude distribution in various sectors, the Fourier coefficient can be further accumulated from a single switching period to the whole fundamental period. Thereafter, the fundamental and harmonic components of the converter voltage can be deduced.

Since the majority of the converter fundamental current flows into the power grid, the branch of the filter capacitor can be regarded as an open circuit as shown in Fig.3(a). Under the super-synchronous and sub-synchronous operation modes, the grid-connected converter generates and absorbs the active power, respectively. The vector diagram between the converter voltage and grid voltage can be found with the voltage drop across the filter inductor. As the result, the voltage across the filter capacitor can be obtained as well as the capacitor current.

As described in [13], the modulation index and the phase angle of the converter voltage can be deduced based on the converter modeling represented in the dq-reference frame. The FFT analysis of the converter voltage is shown in Fig.4, where the wind speeds

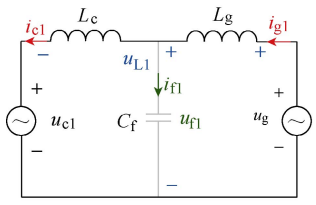

(a) Configuration of the LCL filter

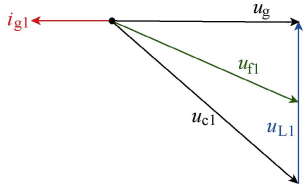

(b) Vector diagram of the LCL filter in the case of the super-synchronous operation

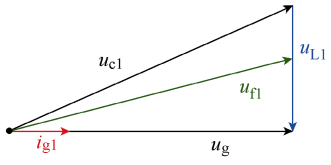

(c) Vector diagram of the LCL filter in the case of the sub-synchronous operation

Fig.3 Relationship between the converter voltage and the filter capacitor electrical stresses

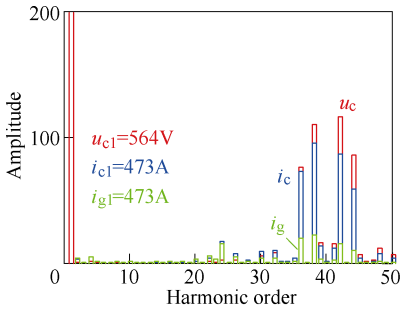

(a) Super-synchronous mode at the wind speed of 12m/s

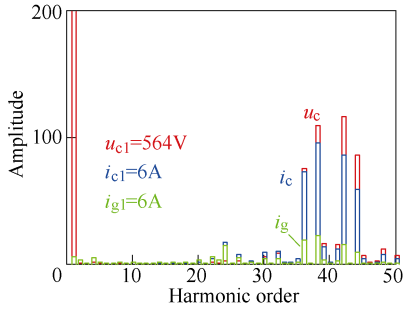

(b) Synchronous mode at the wind speed of 8.4m/s

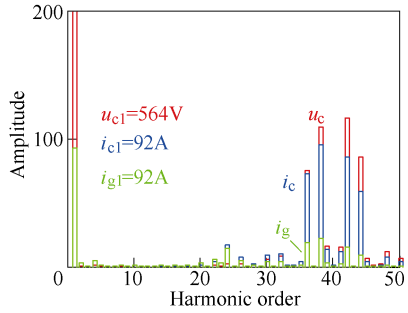

(c) Sub-synchronous

Fig.4 Converter voltage, converter-side current and grid-side current FFT analysis of the grid-connected converter

Table 1 Parameters of A 2MW DFIG system

Parameters	Values
Rated power/ MW	2
Rated amplitude of phase voltage/ V	563
Grid-side inductor/μH	125
Converter-side inductor/μH	125
Filter capacitor/μF	300
DC-link voltage/V	1050
Switching frequency/kHz	2

of 12m/s, 8.4m/s, and 5.9m/s represent the super-synchronous, synchronous, and sub-synchronous operation of the DFIG. It can be observed that, regardless of the operational modes, the fundamental voltage is always 564V, which is similar to the grid voltage due to the negligible voltage drop across the LCL filter. However, the fundamental component of the converter-side current changes considerably at various wind speeds, which becomes the lowest at the synchronous mode due to little active power flowing through the back-to-back power converter. As the LCL filter generally behaves as a low-pass filter, the fundamental component of the grid-side current is the same as the converter-side current.

It is well known that the RMS of the voltage or current is defined as the square root of the mean square,

which consists of both the fundamental component and harmonic components. In addition, as the output power of the wind turbine obeys the maximum power point tracking(MPPT) algorithm[13-14], the relationship between the converter voltage and the wind speed can be established. Based on the FFT analysis of the converter voltage and current, their fundamental, harmonics and RMS values can be obtained as shown in Fig.5 from the cut-in wind speed(4m/s) until the rated wind speed (12m/s).

3.2 Simulation validation

With the harmonic spectrum of the converter-side current and grid-side current, their total harmonic distortions(THDs) can be obtained. As the harmonic component of the capacitor current is dependent on both its amplitude and phase angle, the worst case THD can be roughly estimated by the sum of the converter-side current and the grid-side current[15]. The simulation results of the grid-connected converter are shown in Fig.6, where the harmonic spectrum of the converter

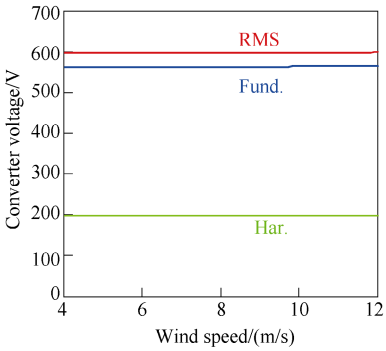

(a) Converter voltage

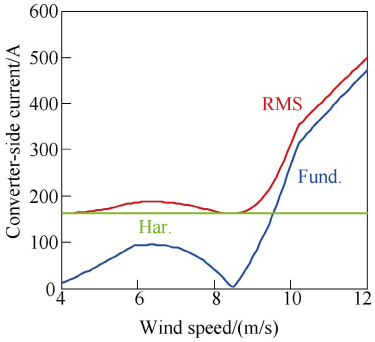

(b) Converter-side current

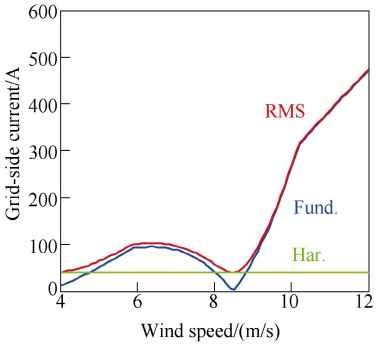

(c) Grid-side current

Fig.5 Analysis of the fundamental, harmonic and RMS components

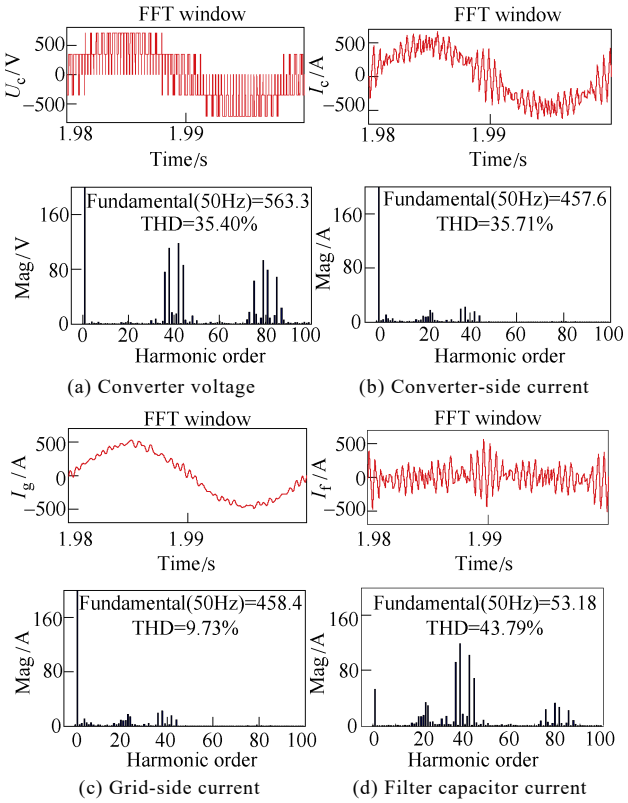

(a) Converter voltage (b) Converter-side current

(c) Grid-side current (d) Filter capacitor current

Fig.6 Simulation results of the grid-connected converter at the wind speed of 12m/s in time and frequency domain

voltage, converter-side current, grid-side current, and the filter capacitor current is investigated. For the converter voltage, its fundamental component and dominant harmonics are consistent with the theoretical calculations as shown in Fig.4(a). Moreover, the fundamental component of the converter-side current and grid-side current is almost the same, and the switching harmonics of the grid-side current are considerably reduced compared with the converter-side converter current. In respect to the capacitor current, it mainly contains the switching harmonics, while the fundamental current is significantly reduced.

Under different loading conditions, the calculated and simulated THDs are summarized and compared in Fig.7. At the wind speed of 12m/s, the calculated fundamental component of the converter-side current and the grid-side current is 1.0pu with their THDs of 34% and 8%, respectively. Moreover, it can be seen that the fundamental component of both the simulated converter-side current and the grid-side current is 0.97pu, and their THDs are 36% and 10%. For the capacitor current, the calculated and the simulated THDs are 43%

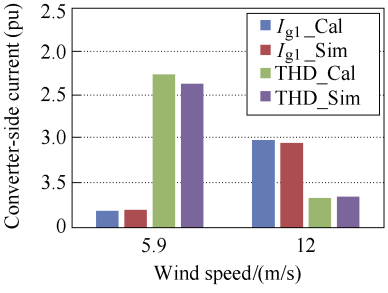

(a) Converter-side current

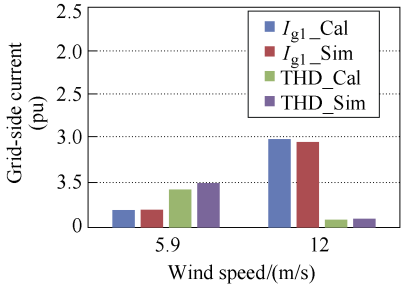

(b) Grid-side current

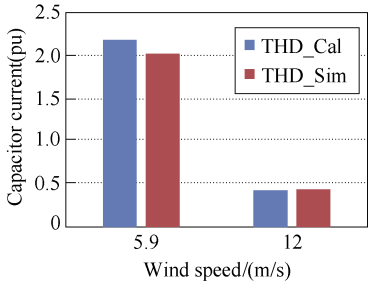

(c) Capacitor current

Fig.7 Harmonic comparison between the calculation(Cal) and simulation(Sim) of filter capacitor current

and 44%, which agree well with each other. At the wind speed of 5.9m/s, it is evident that the fundamental component is considerably reduced due to the lower produced power, while the THD is significantly increased because of the similar harmonic components.

4 Reliability analysis from individual capacitor to capacitor bank

With the information of the lifetime model, the percentile lifetime of the individual capacitor can be converted into its corresponding time-to-failure. Then, the reliability evaluation of the capacitor bank can be analyzed by using the reliability block diagram.

4.1 Capacitor lifetime model

Due to its bipolar operation and ripple current capability, the film capacitor is usually selected to mitigate the PWM harmonics. As the polypropylene loss becomes the main failure mechanism, the rated lifetime of a typical film capacitor is no less than 100,000 hours at 75℃ and dry condition. Moreover, the film capacitor is sensitive to the applied voltage, where the lifetime decreases with an increasing applied voltage. The relationship between the operational hour and the capacitor core temperature as well as the applied voltage is expressed as

$$L_x = L_r \cdot 2^{\frac{T_r - T_c}{10}} \cdot \left(\frac{V_r}{V_x}\right)^{n_1} \tag{2}$$

where L_x denotes the hours to failure used in the real application, while L_r denotes the hours to the failure of the rated voltage V_r, and upper category temperature T_r. The second and third components denote the impact from the core temperature T_c, and the applied voltage V_x. The detailed parameters for the lifetime model are listed in [16], which is graphically shown in Fig.8.

4.2 Mission profile based capacitor lifetime

According to the mission profile of the wind turbine system (e.g. wind speed and ambient temperature), a general procedure to calculate the lifetime of the film capacitor is shown in Fig.9. On the basis of the wind speed, the produced power is predicted by the MPPT curve, and the current and voltage stresses of each capacitor are evaluated with the generator and converter models. By distinguishing the fundamental and switching components of the filter capacitor current, the core temperature of the capacitor can be jointly decided by the core-ambient thermal resistance and the ambient temperature. Together with the applied voltage across the filter capacitor, the lifetime of the individual capacitor is estimated.

With the annual wind speed (Class I) and ambient temperature with the sample rate of 1 hour as shown in Fig.10(a), the ripple current and the annual accumulated damage are shown in Fig.10(b), (c), respectively. It can be seen that the annual damage increases linearly due to the smooth ripple current throughout the year.

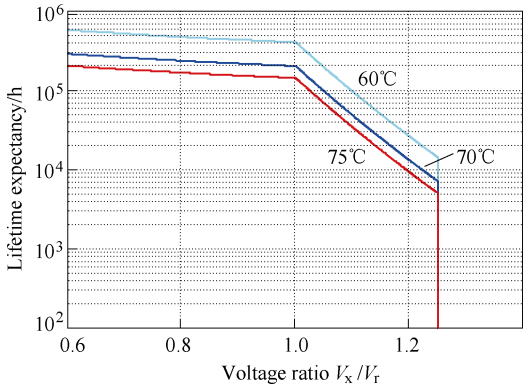

Fig.8 Hour to failure of metalized polypropylene film capacitor with respect to various operating temperatures and applied voltage

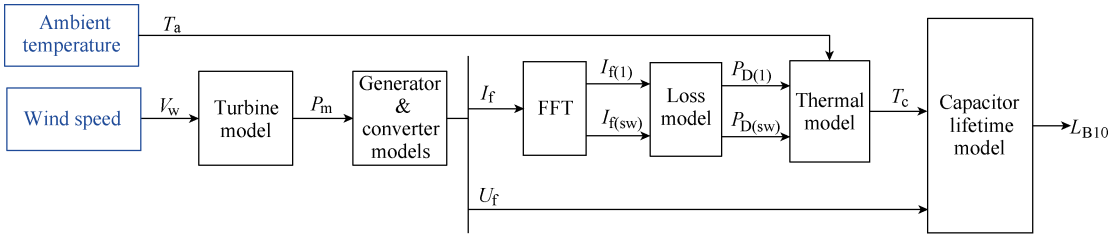

Fig.9 Flowchart to calculate capacitor lifetime from mission profile

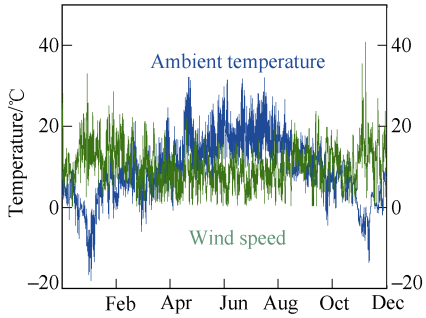

(a) Ambient temperature and wind speed

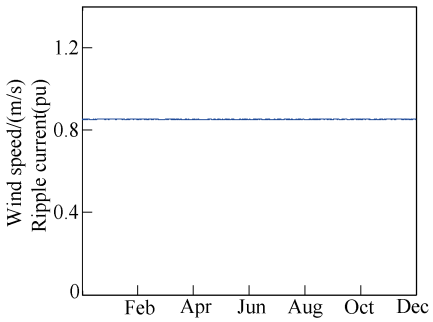

(b) Ripple current

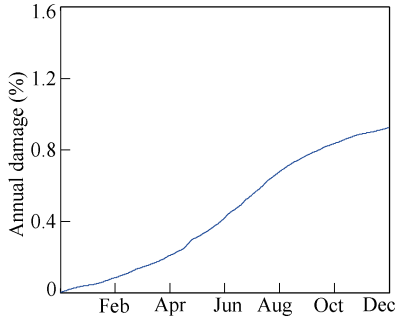

(c) Accumulated damage

Fig.10 Annual profile comparison between the metalized polypropylene film capacitor (MPF-CAP) and the aluminum electrolytic capacitor (Al-CAP)

4.3 Reliability evaluation of the capacitor bank

Considering the tolerance and parameter variation, the B_{10} lifetime of the individual capacitor is converted into its reliability curve along with operation hours. Then, the reliability of the capacitor bank is evaluated with the help of the reliability block diagram.

In order to fulfill the required capacitance and withstand the voltage stress, several capacitors are connected in parallel as a capacitor bank. The detailed structure of the filter capacitor bank is shown in Fig.11(a). Since any failure of the individual capacitor may result in the degraded performance of the capacitor bank, all of the capacitors are connected in series in the reliability block diagram as shown in Fig.11(b).

In order to assess the reliability performance for the capacitor bank, the B_{10} lifetime of the individual capacitor is insufficient, and its time-to-failure distribution, which considers the parameter variations and tolerance uncertainties of the capacitor samples, it is required in order to apply the reliability block calculation. Since the Weibull shape parameter is identical in the case of the same failure mode[8], and

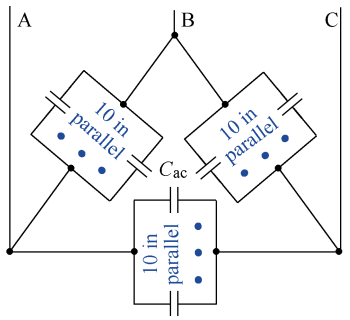

(a) Configuration of the capacitor banks

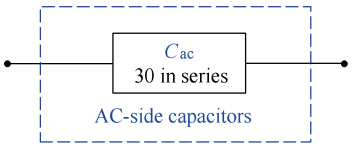

(b) Reliability logics of the whole capacitor bank

Fig.11 Capacitor banks and its reliability

the whole unreliability curve along with the operational hour can be obtained as shown in Fig.12. Moreover, the unreliability curve of the capacitor bank can be deduced from the individual capacitor. Seen from the 15-year designed lifetime of the capacitor bank, the damage of the individual film capacitor becomes 0.0005%, while the capacitor bank damage significantly increases to 0.015%. It is evident that the lifetime relationship between the single capacitor and the capacitor bank is obtained quantitatively. As a large amount of the capacitor cells are applied to form the capacitor bank, the reliability issue of the capacitor bank could become more critical, which results in the optimized capacitor bank design seen from the reliability point of view.

5 Impact of grid fault on filter capacitor stresses

A grid voltage sag is a short duration with the reduced RMS voltage, which can be caused by a short circuit, overload or starting of electric motors. Therefore, the LVRT (Low Voltage Ride Through – also known as FRT-Fault Ride Through) has become a crucial feature of the wind turbine control system. Different LVRT requirements of the stay-connected time duration are defined in Fig.13[17-18].

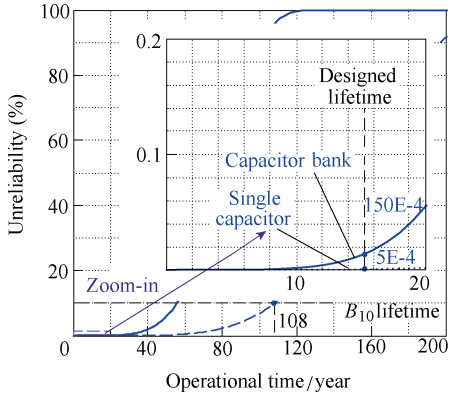

Fig.12 Unreliability curve from the single capacitor to the capacitor bank

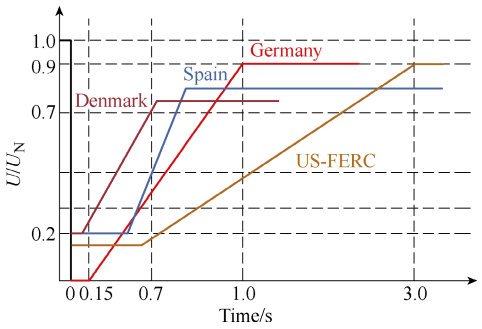

Fig.13 LVRT requirements of wind power systems in different countries

During the LVRT operation, the grid-side components, such as three-phase filtering capacitors, are more severely stressed with voltage and current, which could raise the failure rate of the grid-side passive components. More severely, the asymmetric three-phase capacitor parameters (e.g., capacitance, parasitic inductance) may introduce circulating current in the three-phase capacitor bank, which increases the capacitor hot-spot temperature and accelerates the degradation or catastrophically fail the capacitors. Therefore, the investigation of the electrical stresses of three-phase filter capacitors under grid fault operation is necessary.

In order to clearly define the reliability issue, a three-phase filter capacitor in a 2MW DFIG wind turbine application is studied. The filter capacitor bank with delta connections and asymmetrical parameters are used for investigation. The rated RMS voltage is 730V and the rated current is 50A. The capacitance for phase *a* and *b* is 75μF, the ESR is 1.1mΩ and equivalent series inductance(ESL) is 135nH. Different from that, the measured parameters for phase *c* are 65μF capacitance, 2.2mΩ ESR and 220nH ESL. As a comparable study case, the simulation waveforms of the three-phase capacitor voltage and current with the normal operation are shown in Fig.14(a). Both the voltage and current are stable and within the rated value. Different from that, when a voltage drop to zero for 0.15 second is applied at the grid, the capacitor current and voltage are distorted significantly in a short period as shown in Fig.14(b). It can be seen that: ① The maximum voltage is more than 2 times of the rated one, which may result in catastrophic failure depending on the duration.; ② The maximum current in this period is more than 7 times of the rated maximum current, which could raise the hot-spot temperature and accelerate the degradation process of the capacitors.

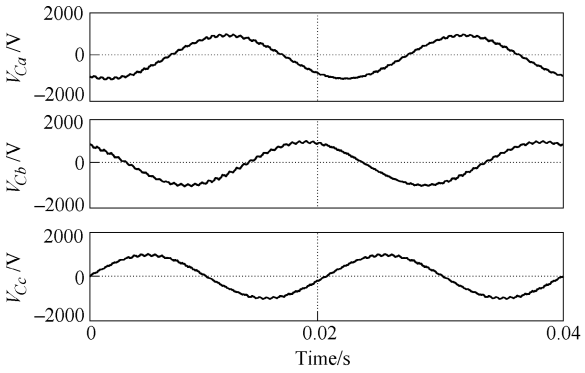

(a) Capacitor voltage waveforms under normal operation

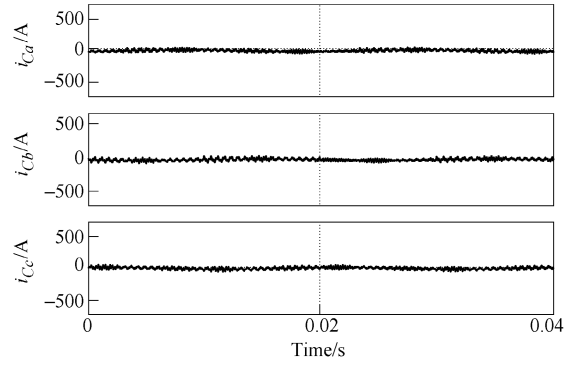

(b) Capacitor current waveforms under normal operation

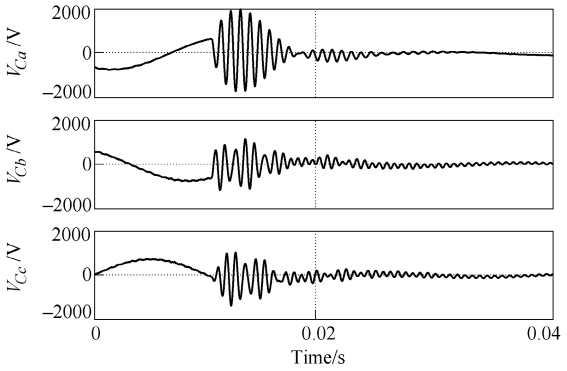

(c) Capacitor voltage waveforms under LVRT

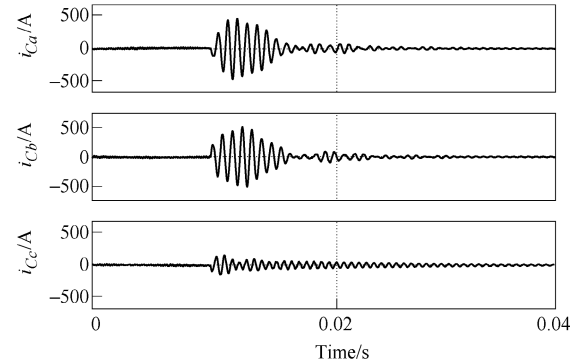

(d) Capacitor current waveforms under LVRT

Fig.14 Three-phase filter capacitor waveforms under normal and LVRT operation

6 Conclusion

Aiming for the grid-connected inverter used in the wind power system, a reliability analysis method of the LCL filter capacitor bank is presented in this paper. According to the converter modulation scheme and the LCL filter impedance characteristic, the electrical stresses(e.g. ripple current, voltage) of the filter capacitor are analytically calculated. By doing so, the annual mission profile(e.g., the wind speed, ambient temperature) is translated into the long-term thermal stress of the filter capacitor, which facilitates its percentile lifetime prediction. Considering the parameter variations among capacitors, the Weibull function based time-to-failure distribution of the single capacitor can further be converted into the filter capacitor bank reliability by using the reliability block diagram. A case study on a 2MW wind turbine system demonstrates that lifetime relationship between the single capacitor and the capacitor bank is obtained quantitatively. Moreover,

the asymmetrical parasitic parameters impact on the electrical stress of the filter capacitor is also investigated, which illustrates that the transient capacitor current and voltage could become multiple times higher compared to the normal operation.

References

[1] F. Blaabjerg, and K. Ma, "Future on power electronics for wind turbine systems," *IEEE Journal of Emerging and Selected Topics in Power Electronics*, vol. 1, no. 3, pp. 139-152, Sept. 2013.

[2] A. Reznik, M. Simoes, A. Al-Durra, and S. Muyeen, "LCL filter design and performance analysis for grid-interconnected systems," *IEEE Trans. on Industry Applications*, vol. 50, no. 2, pp. 1225-1232, Mar. 2014.

[3] Zhiwei Li, Hua Li, Fuchang Lin, Yaohong Chen, and De Liu, "Lifetime prediction of metallized film capacitors based on capacitance loss," *IEEE Trans. on Plasma Science*, vol. 41, no.5, pp. 1313-1318, May 2013.

[4] B. Karanayil, V. G. Agelidis, and J. Pou, "Performance evaluation of three-phase grid-connected photovoltaic inverters using electrolytic or polypropylene film capacitors," *IEEE Trans. on Sustainable Energy*, vol. 5, no. 4, pp. 1297-1306, Oct. 2014.

[5] K. Abdennadher, P. Venet, G. Rojat, J. M. Retif, and C. Rosset, "A realtime predictive-maintenance system of aluminum electrolytic capacitors used in uninterrupted power supplies," *IEEE Trans. on Industry Applications*, vol. 46, no. 4, pp. 1644-1652, Jul. 2010.

[6] A. Lahyani, P. Venet, G. Grellet, and P. J. Viverge, "Failure prediction of electrolytic capacitors during operation of a switch-mode power supply," *IEEE Trans. on Power Electronics*, vol. 13, no. 6, pp. 1199-1207, Nov. 1998.

[7] M. L. Gasperi, "Life prediction modeling of bus capacitors in ac variable frequency drives," *IEEE Trans. on Industry Applications*, vol. 41, no. 6, pp. 1430-1435, Nov. 2005.

[8] D. Zhou, H. Wang, and F. Blaabjerg, "Mission profile based system-level reliability analysis of DC/DC converters for a backup power application," *IEEE Trans. on Power Electronics*, vol. 33, no. 9, pp. 8030-8039, Sept. 2018.

[9] H. Oh, B. Han, P. McCluskey, C. Han, and B. D. Youn, "Physics-of-failure, condition monitoring, and prognostics of insulated gate bipolar transistor modules: a review," *IEEE Trans. on Power Electronics*, vol. 30, no. 5, pp. 2413-2426, May. 2015.

[10] L. Malesani, L. Rossetto, P. Tenti, and P. Tomasin, "AC/DC/AC PWM converter with reduced energy storage in the DC link," *IEEE Trans. on Industry Applications*, vol. 31, no. 2, pp. 287-292, Mar. 1995.

[11] M. Liserre, F. Blaabjerg, and S. Hansen, "Design and control of an LCL-filter-based three-phase active rectifier," *IEEE Trans. on Industry Applications*, vol. 41, no. 5, pp. 1281-1291, Sep. 2005.

[12] V. H. Prasad, "Analysis and comparison of space vector modulation schemes for three-leg and four-leg voltage source inverters," *Master dissertation*, Virginia Tech, Blacksburg, USA, 1997.

[13] D. Zhou, F. Blaabjerg, M. Lau, and M. Tonnes, "Optimized reactive power flow of DFIG power converters for better reliability performance considering grid codes," *IEEE Trans. on Industrial Electronics*, vol. 62, no. 3, pp. 1552-1562, Mar. 2015.

[14] D. Zhou, F. Blaabjerg, T. Franke, M. Tonnes, and M. Lau, "Comparison of wind power converter reliability with low-speed and medium-speed permanent-magnet synchronous generators," *IEEE Trans. on Industrial Electronics*, vol. 62, no. 10, pp. 6575-6584, Oct. 2015.

[15] J. W. Kolar, and S. D. Round, "Analytical calculation of the RMS current stress on the DC-link capacitor of voltage-PWM converter systems," *IEE Proceedings - Electric Power Applications*, vol. 153, no. 4, pp. 535-543, July 2006.

[16] "Aluminum can power film capacitors for PFC and AC filter," *KEMET datasheet*, 2007.

[17] M. Tsili, and S. Papathanassiou, "A review of grid code technical requirements for wind farms," *IET on Renewable Power Generation*, vol. 3, no. 3, pp. 308-332, Sep. 2009.

[18] Y. Yang, F. Blaabjerg, and Z. Zou, "Benchmarking of grid fault modes in single-phase grid-connected photovoltaic systems," *IEEE Trans. Ind. Appl.*, vol. 49, no. 5, pp. 2167-2176, Sept. 2013.

Dao Zhou received the B.S. from Beijing Jiaotong University, Beijing, China, in 2007, the M. S. from Zhejiang University, Hangzhou, China, in 2010, and the Ph.D. from Aalborg University, Aalborg, Denmark, in 2014, all in electrical engineering.

Since 2014, he has been with Department of Energy Technology, Aalborg University, where currently he is an Assistant Professor. His research interests include modeling, control, and reliability of power electronics in renewable energy application. Dr. Zhou received a few IEEE Prize Paper Awards.

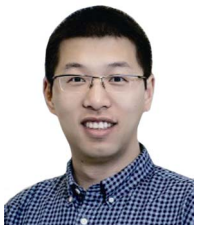

Haoran Wang received the B.S. and M.S. degrees in control science and engineering from Wuhan University of Technology, Wuhan, China, in 2012 and 2015, respectively. He is currently a PhD fellow in Center of Reliable Power Electronics(CORPE), Aalborg University, Aalborg, Denmark. From Aug. 2013 to Sep. 2014, he was research assistant with the Department of Electrical Engineering, Tsinghua University, Beijing, China. He was a Visiting Scientist with the ETH Zurich, Switzerland, from Dec. 2017 to Apr. 2018.

Huai Wang received the B.E. degree in electrical engineering, from Huazhong University of Science and Technology, Wuhan, China, in 2007 and the Ph.D. degree in power electronics, from the City University of Hong Kong, Hong Kong, in 2012. He is currently an Associate Professor at the Center of Reliable Power Electronics(CORPE), aalborg university, aalborg, denmark. He was a Visiting Scientist with the ETH Zurich, Switzerland, from Aug. to Sep. 2014, and with the Massachusetts Institute of Technology (MIT), USA, from Sep. to Nov. 2013. He was with the ABB Corporate Research Center, Switzerland, in 2009. His research addresses the fundamental challenges in modelling and validation of power electronic component failure mechanisms, and application issues in system-level predictability, condition monitoring, circuit architecture, and robustness design.

Dr. Wang received the Richard M. Bass Outstanding Young Power Electronics Engineer Award from the IEEE Power Electronics Society in 2016, and the Green Talents Award from the German Federal Ministry of Education and Research in 2014. He is currently the Award Chair of the Technical Committee of the High Performance and Emerging Technologies, IEEE Power Electronics Society, and the Chair of IEEE PELS/IAS/IE Chapter in Denmark. He serves as an Associate Editor of IET power electronics, IEEE journal of emerging and selected topics in power electronics, and IEEE transactions on power electronics.

Frede Blaabjerg was with ABB-Scandia, Randers, Denmark, from 1987 to 1988. From 1988 to 1992, he got the Ph.D. degree in Electrical Engineering at Aalborg University in 1995. He became an Assistant Professor in 1992, an Associate Professor in 1996, and a Full Professor of power electronics and drives in 1998. From 2017 he became a Villum Investigator.

His current research interests include power electronics and its applications such as in wind turbines, PV systems, reliability, harmonics and adjustable speed drives. He has published more than 500 journal papers in the fields of power electronics and its applications. He is the co-author of two monographs and editor of 6 books in power electronics and its applications.

He has received 24 IEEE Prize Paper Awards, the IEEE PELS Distinguished Service Award in 2009, the EPE-PEMC Council Award in 2010, the IEEE William E. Newell Power Electronics Award 2014 and the Villum Kann Rasmussen Research Award 2014. He was the Editor-in-Chief of the IEEE transactions on power electronics from 2006 to 2012. He has been Distinguished Lecturer for the IEEE Power Electronics Society from 2005 to 2007 and for the IEEE Industry Applications Society from 2010 to 2011 as well as 2017 to 2018. He is nominated in 2014, 2015, 2016 and 2017 by Thomson Reuters to be between the most 250 cited researchers in Engineering in the world. In 2017 he became Honoris Causa at University Politehnica Timisoara(UPT), Romania.